Energy & Environmental Science

ROYAL SOCIETY OF CHEMISTRY

COMMUNICATION

View Article Online
View Journal

Cite this: DOI: 10.1039/d0ee00342e

Received 3rd February 2020,
Accepted 26th March 2020

DOI: 10.1039/d0ee00342e

rsc.li/ees

Determining the limiting factor of the electrochemical stability window for PEO-based solid polymer electrolytes: main chain or terminal –OH group?†

Xiaofei Yang,[a] Ming Jiang,[b] Xuejie Gao,[a] Danni Bao,[c] Qian Sun,[a] Nathaniel Holmes,[a] Hui Duan,[a] Sankha Mukherjee,[b] Keegan Adair,[a] Changtai Zhao,[a] Jianwen Liang,[a] Weihan Li,[a] Junjie Li,[a] Yang Liu,[c] Huan Huang,[c] Li Zhang,[d] Shigang Lu,[d] Qingwen Lu,[a] Ruying Li,[a] Chandra Veer Singh *[b] and Xueliang Sun *[a]

Due to higher energy density, high-voltage all-solid-state lithium batteries (ASSLBs) have attracted increasing attention. However, they require solid-state electrolytes (SSEs) with wide electrochemical stability windows (ESW, typically >4.2 V) and high-stability against the Li anode. Nevertheless, poly(ethylene oxide) (PEO), the most widely used solid polymer electrolyte (SPE), can't tolerate a high-voltage over 4 V. Whether the main chain (–C–O–C–) or the terminal hydroxide group (–OH) is the limiting factor for the narrow ESW remains unknown. Herein, poly(ethylene glycol) (PEG) and poly(ethylene glycol)-dimethyl ether (PEGDME) with different terminal groups are selected to answer this question. The results show that the reactive terminal –OH group is the limiting factor towards applicability against high voltage and the Li anode. Replacing –OH with more stable $-OCH_3$ can significantly extend the ESW from 4.05 to 4.3 V, while improving the Li-anode compatibility as well (Li–Li symmetric cells stably run for 2500 h at 0.2 mA cm^{-2}). Its practical application is further proved by developing PEGDME-based ASSLB pouch cells. The 0.53 mA cm^{-2} Li–$LiFePO_4$ and 0.47 mA h cm^{-2} Li–$LiNi_{0.5}Mn_{0.3}Co_{0.2}O_2$ cells demonstrated high capacity retention of 97% and 90% after 210 cycles and 110 cycles, respectively. This work offers a new strategy for PEO-based high-voltage ASSLB development by changing the unstable terminal groups.

Broader context

High-voltage all-solid-state Li batteries using solid polymer electrolytes have been regarded as promising next-generation batteries in terms of safety and energy density. However, the most widely used solid polymer electrolytes, ether polymer systems, are still challenged by their narrow electrochemical stability windows, which hindered their direct combination with high-voltage cathodes. Searching for the limiting factor and proposing suitable strategies to extend the electrochemical stability windows of ether polymers is of significance to realize high-performance high-voltage all-solid-state Li batteries. In this work, poly(ethylene glycol)-based polymers with the same main chain and different terminal groups are chosen to determine the limiting factor. The results show that the terminal group is the limiting factor and both the electrochemical stability window and electrochemical performance are adjustable *via* changing the terminal group. Replacing the terminal –OH group with the more stable $-OCH_3$ group broadens the electrochemical stability window from 4.05 V to 4.3 V and improves the Li stability. This work opens a new window for designing high-voltage all-solid-state batteries.

In response to the demand for safe, energy-dense electrochemical energy storage, all-solid-state lithium batteries (ASSLBs) have received extensive attention.[1–5] The solid-state electrolyte (SSE) plays dual roles in this model, transferring Li^+ as well as separating the anode and cathode. An ideal SSE should possess the following characteristics: (1) high ionic conductivity (over 10^{-4} S cm^{-1} at operating temperatures); (2) Li dendrite suppression capabilities; (3) low cost, high flexibility and facile large-scale production to meet the requirements of pouch cells; (4) an extended electrochemical stability window (ESW > 4.2 V to be suitable for $LiCoO_2$ (LCO) and $LiNi_xMn_yCo_{1-x-y}O_2$ (NMC)); and (5) excellent chemical/electrochemical stability against Li metal, oxygen and moisture.[6,7] At this point in time, the fabrication of large-scale oxide and sulfide-based SSE thin pallets/films remains challenging and too costly to be practical. Solid polymer electrolytes (SPEs) represent one of the most promising candidates to address these challenges as we work toward the development of ASSLB pouch cells.[6,8–13]

Poly(ethylene oxide) (PEO) is currently the most widely used SPE, but its narrow electrochemical stability window (ESW, less than 4 V) restricts its combination with high-voltage cathodes, which remarkably limits the energy density improvements of PEO SPE-based ASSLBs.[14] Recently, the widely adopted strategies to realize PEO-based SPEs in high voltage ASSLBs have been introducing another high voltage-resistant SPE towards the

[a] Department of Mechanical and Materials Engineering, University of Western Ontario, London, Ontario, N6A 5B9, Canada. E-mail: xsun9@uwo.ca
[b] Department of Materials Science and Engineering, University of Toronto, Toronto, Ontario, M5S 3E4, Canada. E-mail: chandraveer.singh@utoronto.ca
[c] Glabat Solid-State Battery Inc., 700 Collip Circle, London, ONN6G 4X8, Canada
[d] China Automotive Battery Research Institute, Beijing, 100088, P. R. China

† Electronic supplementary information (ESI) available. See DOI: 10.1039/d0ee00342e

cathode and building kinetically stable interfaces at the cathode surface.[15–18] For instance, a PEO/poly(*N*-methyl-malonic amide) (PMA) double-layered SPE was developed by J. B. Goodenough and his co-workers to stabilize the anode/cathode and implemented in a Li–LCO ASSLB operating up to 4.25 V.[16] In another study, Chen's group introduced a $Li_{1.4}Al_{0.4}Ti_{1.6}(PO_4)_3$ coating on LCO to suppress the oxidation of the PEO SPE.[18] The assembled Li–LCO ASSLB achieved 93% discharge capacity retention after 50 cycles with a high charging cut-off voltage of 4.2 V. Very recently, Cui's group extended the usage electrochemical window of PEO *via* lithium salt design.[17] They found that $Li[(CF_3)_3COBF_3]$ promoted formation of a solid–electrolyte interlayer on the anode surface and another cathode–electrolyte interface on the cathode, thus realizing the usage of PEO in a Li–LCO ASSLB at 4.3 V. Despite these great achievements, the factor that limits the improvement of PEO's ESW remains relatively unknown and thus it is still quite challenging to directly combine PEO SPEs with high-voltage cathodes.

It is well-known that the PEO polymer contains a main chain (–C–O–C–) and terminal hydroxide groups (–OH), but which of the two is the limiting factor for the narrow ESW remains a mystery. Interestingly, some ether chain-containing cross-linked SPEs with eliminated –OH groups exhibit extended ESWs.[19–21] For instance, Kim's group developed a cross-linked SPE *via* photo-polymerizing poly(ethylene ether carbonate) and tetraethylene-glycol diacrylate. They showed that the cross-linked SPE possesses an extended ESW of 4.9 V, which is 0.4 V higher than the PEO electrolyte, enabling the $Li/LiNi_{0.6}Co_{0.2}Mn_{0.2}O_2$ SSLB to stably cycle for over 100 cycles with a capacity retention of 90.2% under an operating voltage window of 3.0–4.3 V.[21] Moreover, such an ether-chain-containing polymer as poly(ethylene glycol)dimethyl ether (PEGDME) has been widely applied as a plasticizer to improve the ionic conductivities of SPEs. Meanwhile, the PEGDME plasticizer has demonstrated its high stability under high voltages over 4.2 V and enabled assembled cells with excellent cycling stability.[22–24] The above findings suggested that the terminal –OH may be responsible, instead of the ether chain (–C–O–C–), for limiting the ESW range of SPEs. In other words, if we can clarify this hypothesis, more high-voltage-resistant ether SPEs can be developed by modifying the terminal –OH with more stable groups. Moreover, the Li anode stability can also be improved concurrently by eliminating the instability of the –OH group against the Li anode.

Herein, poly(ethylene glycol) (PEG) and PEGDME with different terminal groups (–OH *vs.* $–OCH_3$, Fig. S1, ESI†) are chosen as representatives to investigate the effect of the terminal group on the Li anode stability and ESW, where PEG possesses the same molecular structure as PEO. The results showed that in a dual-salt system (lithium bis(trifluoromethanesulfonyl)-imide (LiTFSI) and lithium bis(fluorosulfonyl)imide (LiFSI)), the PEGDME-based SPE delivered an extended ESW of 4.3 V (as illustrated in Fig. 1a), which is 0.25 V higher than its counterpart (PEG, illustrated in Fig. 1b). Moreover, after eliminating the highly active –OH group, the PEGDME-based SPE shows excellent Li anode stability, enabling the Li–Li symmetric cells to stably run for over 2500 cycles at 0.2 mA cm^{-2}, while sharply increasing the overpotential for the PEG SPE-based Li–Li symmetric cell. Both the extended ESW

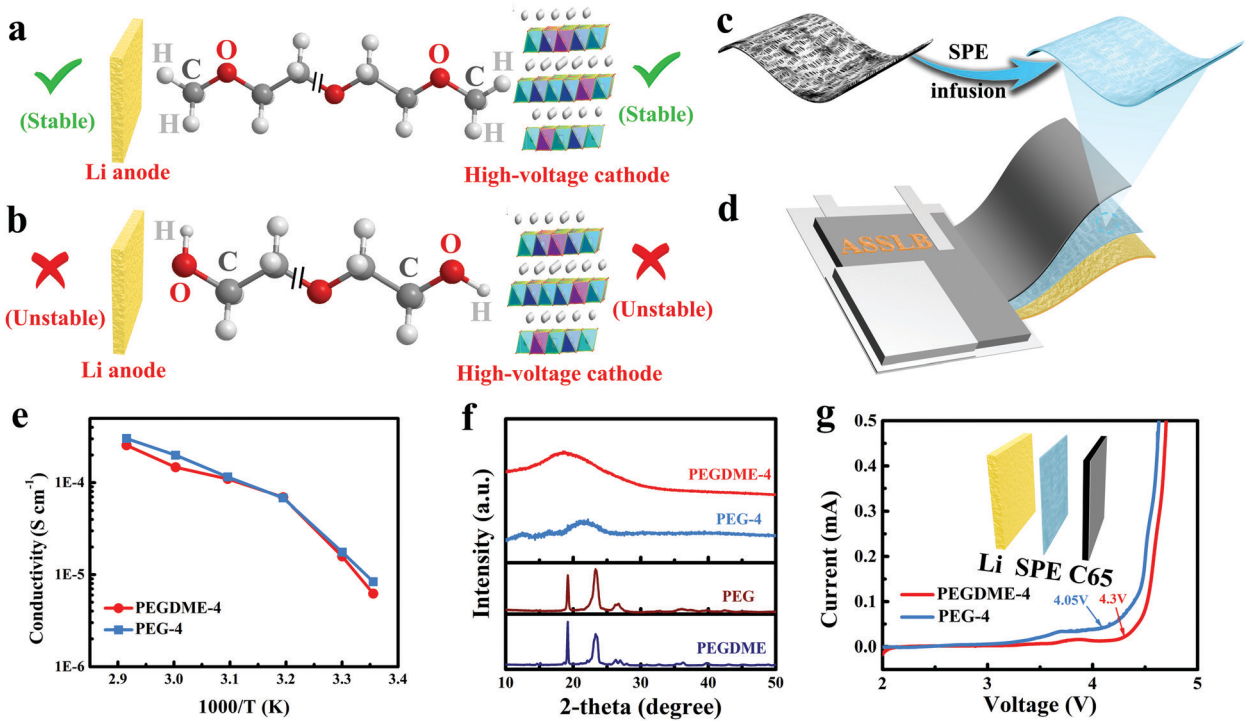

Fig. 1 Schematic illustration of the (a) PEGDME and (b) PEG response to the Li anode and a high voltage. (c) PEGDME (PEG)-based SPE fabrication by infusing the polymer electrolyte into a Celgard 3501 separator. (d) Schematic illustration of a pouch cell assembled with the as-prepared SPE. (e) Ionic conductivities, (f) XRD patterns and (g) electrochemical stability windows of PEGDME-4 and PEG-4 SPEs.

and enhanced Li stability confirm our hypothesis that the reactive –OH group is the limiting factor for the narrow ESW and poor Li stability. Besides the above fundamental understanding, the as-prepared SPEs present huge potential for practical application due to their facile, economic and scalable fabrication process as well as excellent electrochemical performance. The assembled 0.53 mA cm^{-2} Li–$LiFePO_4$ (LFP) and 0.47 mA h cm^{-2} Li–$LiNi_{0.5}Mn_{0.3}Co_{0.2}O_2$ (NMC532) ASSLB pouch cells demonstrate high capacity retention of 97% and 90% after 210 cycles and 110 cycles, respectively. This work provides the fundamental understanding needed for fabrication of high-voltage-resistant SPEs and their practical application in pouch cells.

As illustrated in Fig. 1c, the SPEs are produced through a simple melt-infusion process in which the melted PEGDME (or PEG, M_n = 2000) electrolyte (with dissolved LiTFSI and/or LiFSI) is impregnated into a porous Celgard 3501 separator (Fig. S2b and S3, ESI†) at a temperature of 120 °C (Fig. S2a, ESI†). This process takes only 5–10 s. Considering that the fabrication process is facile, economic and scalable, the as-prepared SPEs have the potential to be used in pouch cells (Fig. 1d). LiTFSI plays an important role in reducing the crystallinity of PEGDME and improving the ionic conductivity (Fig. S4a, ESI†), while LiFSI is helpful to produce a LiF-rich SEI on the Li metal surface (Fig. S4b, ESI†). This LiF-rich SEI promotes uniform Li deposition and suppresses Li dendrite growth.[25,26] The dual-salt system chosen here is to achieve high ionic conductivity and high Li dendrite suppression capability simultaneously, which is required to accurately evaluate the intrinsic properties of polymers by eliminating the effect of Li dendrites and Li^+ transport. PEG and PEGDME with different LiTFSI/LiFSI ratios are labeled as PEGDME (PEG)-*x*, where *x* is the ratio of LiTFSI/LiFSI. PEGDME (PEG) with single LiTFSI and LiFSI is labeled as PEGDME (PEG)-10 and PEGDME (PEG)-0 SPEs, respectively. The EG/Li ratio is controlled at 12/1 due to its solid state at room temperature (Fig. S5, ESI†).

To confirm the influence of each lithium salt component, the ionic conductivity, XRD pattern and relative ESWs of the PEGDME-*x* SPEs are investigated. Fig. S6a (ESI†) displays the results of the ionic conductivity testing. It can be seen that the PEGDME-10 and PEGDME-4 SPEs show a similar ionic conductivity of $\sim 1.5 \times 10^{-4}$ S cm^{-1} at 60 °C. Increasing the ratio of LiFSI further, the ionic conductivity falls to such an extent that the ionic conductivity of PEGDME-0 is 3.1×10^{-5} S cm^{-1}, almost one fifth that of the PEGDME-10 and PEGDME-4 SPEs. The XRD results shown in Fig. S6b (ESI†) provide an indication as to the probable reason for this result. The PEGDME-10 and PEGDME-4 SPEs possess an amorphous structure and only weak peaks belonging to Celgard 3501 are detected. In contrast, when the LiTFSI/LiFSI ratio is reduced below 1/1, the peaks belonging to PEGDME suggest increased crystallinity of PEGDME in the PEGDME-1 and PEGDME-0 SPEs. The increased crystallinity of PEGDME in the PEGDME-1 and PEGDME-0 SPEs is largely responsible for the lower ionic conductivities.[6,27] These results confirm the role of LiTFSI in reducing the crystallinity of PEGDME, thereby improving the ionic conductivity. For comparison, the ionic conductivities of the PEGDME-4 and PEG-4 SPEs are also tested. Due to the similar molecular weight of PEGDME and PEG, with the same Li salt components both SPEs present an amorphous structure (according to the XRD patterns in Fig. 1f), resulting in a similar ionic conductivity of $\sim 1.5 \times 10^{-4}$ S cm^{-1} at 60 °C (Fig. 1e). In this regard, we can exclude the effect of ionic conductivity and Li^+ transport in the following Li anode stability and high-voltage-resistant testing.

The ESW testing in Fig. 1g and Fig. S7 (ESI†) demonstrates the high-voltage compatibility of PEGDME, as compared to PEG. The electrochemical stability windows were tested with two cell types: Li|SPE|C65 and Li|SPE|Al foil. Fig. S7 (ESI†) shows that the PEGDME-*x* SPEs with different Li salt components have the same ESW of 4.3 V in the C65 cell and 4.7 V in the Al foil cell. These results indicate that the ESWs of the SPEs are mainly determined by the PEGDME polymer, while Li salts having a negligible effect. The difference in the measured ESW between the two cell types can be attributed to the more reactive C65, which promotes the decomposition of the SPEs. Considering that the carbon additive is an indispensable component in cathode materials, the ESW obtained from the Li|SPE|C65 cell is more reasonable. For comparison, the PEG-4 SPE is also tested in the Li|SPE|C65 cell, and the result is shown in Fig. 1g. It is found that the PEG-4 SPE can only tolerate a voltage up to 4.05 V, and therefore does not fulfill the requirements for high-voltage ASSLBs. Due to the same Li salts in PEGDME-4 and PEG-4, the different ESWs can be attributed to the different polymers in the two SPEs. We can, therefore, conclude that modifying the terminal –OH group in PEG with $–OCH_3$ extends the ESWs of SPEs. To further confirm the effect of the terminal group, the ESWs of poly(ethylene glycol) distearate (PEG-distearate) and another two PEG polymers with different molecular weights of 400 and 20 000 are investigated. As shown in Fig. S8 (ESI†), decreasing or increasing the molecular weight of PEG, indicating more or less terminal –OH groups, led to narrowed and extended ESWs of 3.35 V and 4.23 V. Replacing the terminal –OH group with $–OCO(CH_2)_{16}CH_3$ can also achieve an ESW of 4.3 V (Fig. S9, ESI†), suggesting that it is a universal method to extend the ESW *via* changing the unstable terminal –OH group.

The roles of LiFSI in stabilizing the Li anode are studied by cycling Li–Li symmetrical cells (Li foil with 1.0 cm diameter) with PEGDME-*x* at 60 °C. The current density is controlled at 0.2 mA cm^{-2} and each half cycle is 1 h. As shown in Fig. 2a and Fig. S10 (ESI†), due to the higher ionic conductivity of the PEGDME-10 and PEGDME-4 SPEs, the cells assembled with the PEGDME-10 and PEGDME-4 SPEs present lower overpotentials of around 170 mV. More importantly, it should be noted that the overpotential of the cell assembled with PEGDME-10, which has no LiFSI salt in the SPE, gradually climbed to almost 520 mV after 920 h. The overpotential then suddenly drops to 0 V (Fig. S10, ESI†), suggesting the occurrence of a short-circuit.[28,29] This indicates that the single salt LiTFSI cannot prevent Li dendrite growth in spite of its contribution toward improving the ionic conductivity. The LiFSI-based SPE (PEGDME-0) cannot meet the requirements of ASSLBs either. The assembled Li–Li symmetric cells exhibited a high initial overpotential of over 750 mV.

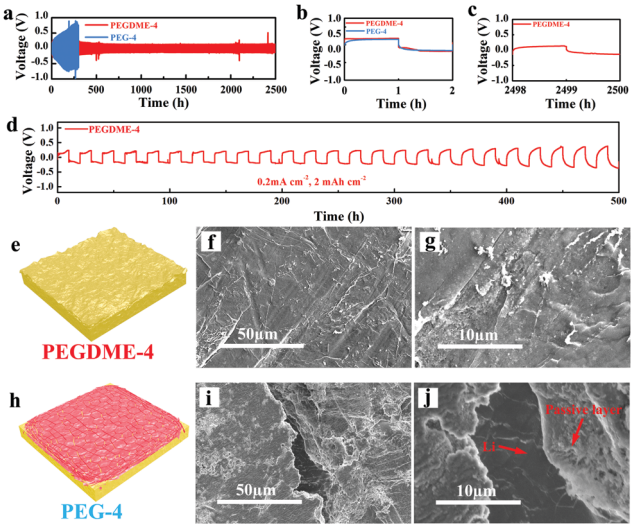

Fig. 2 (a) Cycling performance and (b and c) relative plating/stripping profiles of Li–Li symmetrical cells with PEGDME-4 and PEG-4 at a current density of 0.2 mA cm^{-2} (capacity: 0.2 mA h cm^{-2}). (d) Cycling stability of the Li–Li symmetrical cells assembled with PEGDME-4 with a current density of 0.2 mA cm^{-2} and a capacity of 2 mA h cm^{-2}. (e) Schematic illustration of the Li deposition morphology and (f and g) SEM images of the Li anode in the PEGDME-4 SPE after 50 h. (h) Schematic illustration of the Li deposition morphology and (i and j) SEM images of the Li anode in the PEG-4 SPE after 50 h.

Due to the large bias voltage applied to the cell, the plating/stripping behavior is unstable, and fluctuating plating/stripping profiles and overpotentials follow. After 500 h, intermittent short-circuiting is observed. Clearly, neither single salt LiFSI nor LiTFSI can suppress Li dendrites in ASSLBs.

Interestingly, combining PEGDME with dual salts improves the cycling stability of Li–Li symmetric cells. Li–Li symmetric cells using PEGDME-4 and PEGDME-1 can stably cycle for over 2500 h and 1000 h, respectively (Fig. 2a and Fig. S10, ESI†). Moreover, a negligible increase in overpotential is observed, indicating uniform Li plating and stripping during cycling. The role that LiFSI played in helping to suppress Li dendrite growth can be attributed to the LiF-rich SEI, which promotes uniform Li deposition, and the detailed description can be seen in the ESI† (Fig. S11–S13). Taking both the ionic conductivity and Li plating–stripping performance into consideration, a LiTFSI/LiFSI ratio of 4 is found as the optimal Li salt component, and it is therefore chosen as the Li salt for the following electrochemical performance investigation of PEG and PEGDME.

To study the role of the $-OCH_3$ group in the PEGDME structure in enhancing the Li stability, the PEG-4 SPE is chosen for comparison. As shown in Fig. 2a, the overpotential of the assembled Li–Li symmetric cell shows a sharp, unexpected rise to over 0.8 V after 300 h. Considering the same Li salts in the PEGDME-4 and PEG-4 SPEs, such a huge difference in the Li–Li symmetric cells can be attributed to the more stable $-OCH_3$ group in PEGDME, which enhances the stability of the SPEs against Li anodes. To further confirm that the terminal –OH group is the unstable factor that leads to the increasing overpotential during cycling, Li–Li symmetric cells assembled with the PEG (400)-4 and PEG (20 000)-4 SPEs are also tested under the same conditions. As displayed in Fig. S14 (ESI†), the Li–Li symmetric cell using the PEG (400)-4 SPE presents more instability against the Li anode. The overpotential sharply increases to a cutoff voltage of 5 V in 3 cycles, while the PEG with a molecular weight of 20 000 with fewer –OH groups can stably run for over 300 cycles with a slight overpotential increase. Replacing the terminal –OH group with $-OCO(CH_2)_{16}CH_3$ (PEG-distearate-4 SPE) can also enhance the Li stability and enable the Li–Li symmetric cells to stably run for over 500 cycles (Fig. S15, ESI†). These results can further prove that the –OH group is the unstable group against Li. To understand the ability of PEGDME to stabilize the Li anode, Li–Li symmetric cells using the PEGDME-4 and PEG-4 SPEs were disassembled after 50 hours of cycling. The optical images of the Li anodes are shown in Fig. S16 (ESI†). The Li anode in PEGDME-4 maintains its metallic luster, while the lithium surface becomes dull when paired with the PEG-4 SPE (Fig. S16, ESI†). Inspection of the SEM images reveals that the Li anode in the PEGDME-4 SPE presents a flat surface morphology (Fig. 2e–g), which is maintained for a long cycling time of over 1000 h (Fig. S17a–c, ESI†). In contrast, in the PEG-4 SPE, a passivation layer is formed on the surface of the Li anode (Fig. 2h–j and Fig. S17d and e, ESI†) and the thickness is determined to be 70 μm after 300 h (Fig. S17f, ESI†). This is mainly due to side-reactions between the reactive –OH group in PEG and strongly reducing Li, and they are posited to be the root cause of the poor electrochemical performance of Li–Li symmetric cells. In this regard, we can conclude that replacing the reactive –OH group in PEG with stable $-OCH_3$ or $-OCO(CH_2)_{16}CH_3$ groups is beneficial for stabilizing the Li anode, thus leading to better electrochemical performance of Li–Li symmetric cells. It is well known that high areal capacity is a very important parameter to enable high-energy-density ASSLBs.[29–31] The cycling stability of Li–Li symmetric cells using PEGDME-4 SPE is therefore evaluated under a high capacity of 2 mA h cm^{-2}, with a current density of 0.2 mA cm^{-2}. As shown in Fig. 2d, the Li–Li symmetric cell demonstrates excellent Li plating/stripping performance over 500 h, further highlighting the ability of PEGDME-4 in stabilizing the Li anode.

The role that the $-OCH_3$ group and LiFSI played in stabilizing the Li anode is further verified in Li–LFP ASSLB coin cells. In good agreement with the Li–Li symmetric cells, the electrochemical performance of the Li–LFP coin cells in Fig. S18–S20 (ESI†) demonstrates that PEGDME-4 is the optimal SPE among the PEGDME-*x* series because of the Li dendrite suppression capability as well as the high ionic conductivity, consequently resulting in higher capacity output and better cycling stability. The PEGDME-4-based Li-LFP cell assembled with a 14.5 mg cm^{-2} LFP-loaded cathode exhibits good cycling stability with a high reversible areal capacity of around 1.74 mA h cm^{-2} for 30 cycles (Fig. S21, ESI†), further confirming the effect of the $-OCH_3$ group and LiFSI on stabilizing the Li anode. Further details are provided in the ESI.†

To further explore the effect of $-OCH_3$ on resisting oxidation of PEGDME under a high voltage, NMC532 is chosen as the cathode material to investigate the electrochemical behavior of PEG and PEGDME SPEs based on the optimized LiTFSI/LiFSI ratio of 4. The assembled Li-NMC532 ASSLB coin cells are

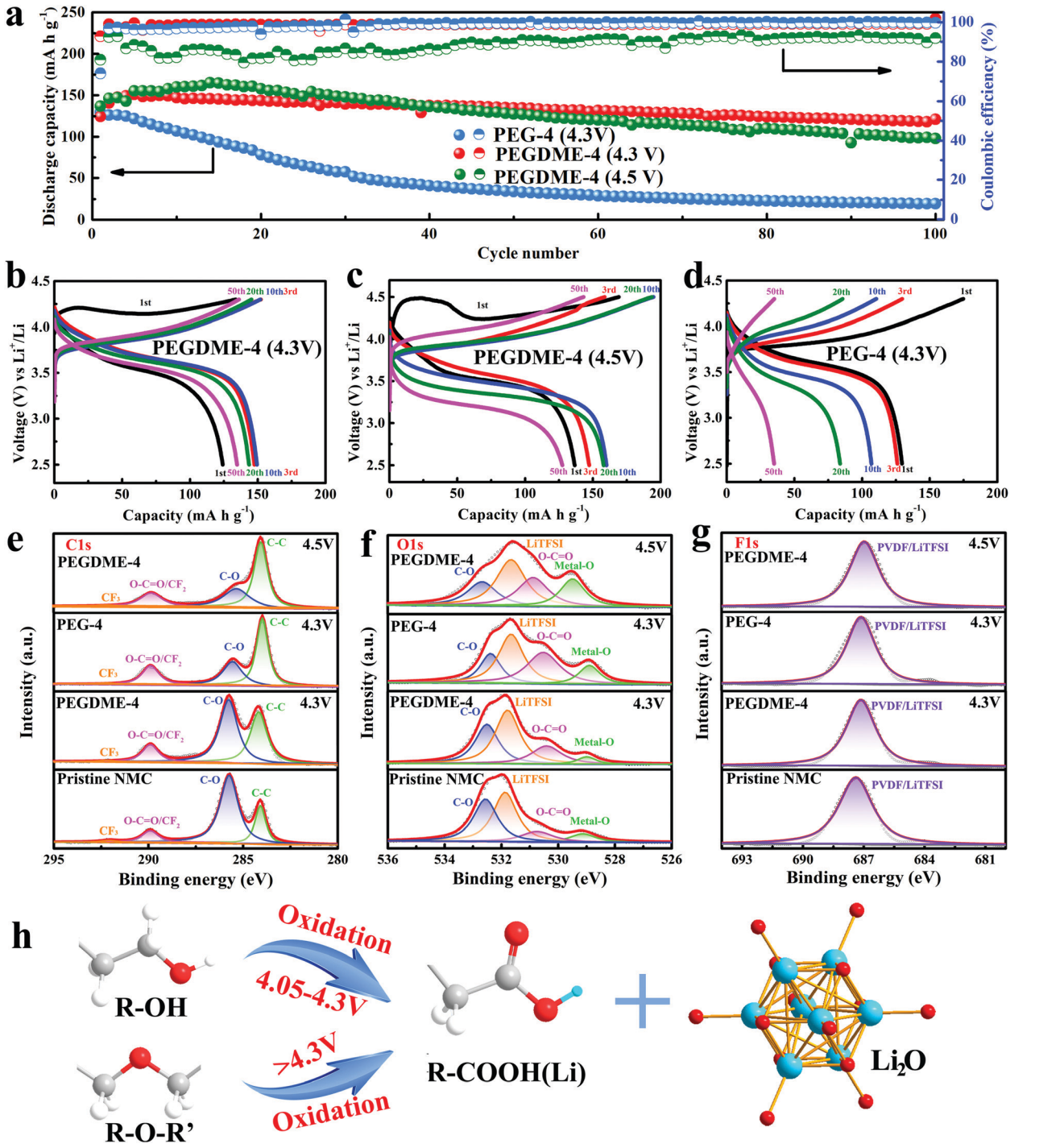

Fig. 3 (a) Cycling performance and (b–d) relative charge–discharge profiles of Li-NMC532 coin cells using PEGDME (PEG)-4 SPEs with operating voltage ranges of 2.5–4.3 V and 2.5–4.5 V (NMC532 loading: 3–4 mg cm^{-2}, current density: 0.2C). (e) C 1s, (f) O 1s and (g) F 1s spectra of (from bottom to top) pristine NMC, NMC using PEGDME-4 at 4.3 V, NMC using PEG-4 at 4.3 V and NMC using PEGDME-4 at 4.5 V. (h) Possible oxidation mechanism of ether-based polymers under high voltages.

tested under voltage windows of 2.5–4.3 V and 2.5–4.5 V. The NMC532 loading is controlled at 3–4 mg cm^{-2} and the C-rate set to 0.2C. As shown in Fig. 3a, the Li-NMC532 cell using PEGDME-4 delivered a reversible capacity of around 150 mA h g^{-1} and a high average coulombic efficiency (CE) of over 99% after a few cycles of activation (voltage window: 2.5–4.3 V). After 100 cycles, a capacity of 121 mA h g^{-1} is maintained. A capacity retention of over 80% and negligible overpotential increase (Fig. 3b) indicate that the PEGDME-4 SPE can tolerate a high voltage of up to 4.3 V. This result is in agreement with the ESW testing using the Li|SPE|C65 cell. Further increasing the charging cut-off voltage to 4.5 V results in poor cycling stability and lower CEs.

At this voltage, the capacity retention is only 59% (165 to 97 mA h g^{-1}) and the average CE is 88%. The fast capacity decay and low CEs are mainly due to the decomposition of PEGDME-4 at a high-voltage of 4.5 V, inhibiting Li^+ transport and increasing the overpotential (Fig. 3c). We, therefore, conclude that the PEGDME-4 SPE can tolerate a voltage of up to 4.3 V and is suitable for high-voltage ASSLBs.[15,17] For comparison, the Li-NMC532 coin cell using the PEG-4 SPE is also tested in the voltage window of 2.5–4.3 V and the results are presented in Fig. 3a and d. Fast capacity decay (from 130 mA h g^{-1} to 19 mA h g^{-1}), low CEs (around 96% in the first 30 cycles) and increased overpotential (Fig. 3d) are observed. The poor electrochemical performance of the PEG-4 SPE-based Li-NMC532 cell can be attributed to the low stability of the PEG-4 SPE toward the Li anode and the high-voltage cathode. Further increasing or decreasing the ratio of the terminal –OH groups *via* adjusting the molecular weight of PEG, significantly changed cycling stability can be seen in Fig. S22 (ESI†). The discharge capacity of the cell using the PEG (400)-4 SPE sharply decays to 16 mA h g^{-1} in 30 cycles, while the cell using the PEG (20 000)-4 SPE retains a capacity of 62 mA h g^{-1} after 100 cycles. Additionally, the electrochemical performance of Li-NMC532 cells assembled with PEG-distearate-4 is also tested in the voltage window of 2.5–4.3 V. As shown in Fig. S23 (ESI†), similar to PEGDME, the PEG-distearate-4-based Li-NMC532 cell demonstrates excellent cycling stability with a capacity around 120 mA h g^{-1} and negligible overpotential increase in charge/discharge profiles over 100 cycles. These results confirm that the ESW and electrochemical performance of PEG-based SPEs are adjustable and greatly affected by the terminal group.

To exclude the impact of the anode part on the battery performance and understand the mechanism behind the improved electrochemical performance by replacing the terminal –OH group with $–OCH_3$, the cells are disassembled after 5 cycles and the cathodes are characterized using X-ray photoelectron spectroscopy (XPS). The surface information collected from XPS in Fig. S24 (ESI†) shows no chemical valence change for the elements of Ni, Co, and Mn during cycling up to 4.3 V and 4.5 V. XPS is also used to investigate C, O, and F surface signals. Fig. 3e shows the C 1s spectra of the pristine NMC cathode and NMC cathode after cycling in PEG-4 (2.5–4.3 V) and PEGDME-4 (2.5–4.3 V and 2.5–4.5 V) SPEs. Four peaks can be observed at 292.1 eV, 290.0 eV, 285.7 eV and 284.1 eV, which can be assigned to CF_3, O–C═O/CF_2, C–O and C–C, respectively.[32] For the pristine NMC cathode, the C–C signals can be assigned to the molecular skeleton of PEGDME and the PVDF binder added during cathode preparation. The CF_3 and CF_2 signals in the C 1s spectra and F 1s spectra (687.4 eV, Fig. 3g) come from LiTFSI and the PVDF binder. The C–O signal in C 1s and O 1s (532.5 eV in Fig. 3f) can be attributed to the ether chain (–C–O–C–) in PEGDME, while the O–C═O (530.7 eV in Fig. 3f) detected in the O 1s spectra can be attributed to the O species on the surface of the pristine NMC. The signal at 531.9 eV in Fig. 3f belongs to LiTFSI.[32] The metal–O signal at 529 eV is due to lattice O in the NMC.[33,34] When the NMC cathode with the PEGDME-4 SPE operates at 4.3 V, all the C, O, and F species show negligible change, where the peak area ratio of (Metal–O + O–C═O)/C–O is kept as 0.82 (similar to the pristine NMC: 0.65), indicating good stability of both the NMC and the PEGDME-4 SPE at 4.3 V. In other words, –C–O–C– is stable against a high voltage of 4.3 V. Of particular interest is that the intensities of C–O and O–C═O/Metal–O (belonging to the formation of Li_2O)[35] appear to be anti-correlated operating in the PEG-4 SPE and the peak area ratio of (Metal–O + O–C═O)/C–O increases to 2.33, indicating that C–O is consumed to form O–C═O/Li_2O. Considering the high-stability of –C–O–C–, the consumption of C–O can be attributed to the oxidation of the –C–OH group in PEG. In other words, the terminal –OH is the limiting factor for the narrow ESW of the PEG-4 SPE. Further operating PEGDME-4 under an elevated voltage of 4.5 V, a similar phenomenon with decreasing C–O intensity and rising O–C═O/Metal–O intensity is presented (the peak area ratio of (Metal–O + O–C═O)/C–O is 2.30), indicating the oxidation of –C–O–C–. Combining with the ESW testing in Fig. 1g, a possible oxidation mechanism under high voltages is assumed and presented in Fig. 3h. The terminal –OH will be oxidized into –COOH (Li) with formation of Li_2O in the voltage window of 4.05–4.3 V, limiting its combination with high-voltage cathodes. Further increasing the voltage to over 4.3 V, the ether chain (–C–O–C–) will be oxidized. That is to say, replacing the terminal –OH group with more stable groups has the potential to extend the ESW of PEO SPEs to 4.3 V.

To gain fundamental insights into the high stability of $–OCH_3$ toward the Li anode and high-voltage, we utilize DFT simulations to understand the interaction of PEGDME and PEG with the Li anode surface under external electric fields (Fig. 4; the molecular models of PEG and PEGDME can be seen in Fig. S25, ESI†). To study the absorption of the molecules over the Li surface, three adsorption sites (top, bridge and parallel) are considered on the Li(100) plane, as the Li(100) surface shows thermodynamic stability due to the lowest surface energy (the methodology and further details can be seen in the ESI,† Fig. S25 and Table S2). As shown in Fig. 4a–f, PEGDME presents stronger adsorption energies compared with its counterpart at all three absorption sites, indicating a more stable interface between the Li anode and PEGDME, and thereby increasing surface wetting and facilitating Li^+ transport.[36] The concept is further confirmed by the adsorption energy study for PEG-distearate. Due to the large steric hindrance effect in the top and bridge model, herein, only the strongest adsorption model (parallel) is investigated. As shown in Fig. S26 (ESI†), PEG-distearate also displays stronger adsorption energy (−2.26 eV) compared with PEG (−2.01 eV). In other words, besides hindering the side reaction with Li, replacing the terminal –OH with more stable end groups is also expected to increase the stability of the Li/SPE interface. The total energy change (ΔE) of PEG and PEGDME as induced by an electric field is further explored (Fig. 4g). During the charging (from 0 V $Å^{-1}$ to 0.2 V $Å^{-1}$) and discharging process (from 0 $Å^{-1}$ to −0.2 V $Å^{-1}$), an increasing ΔE value can be observed, which is caused by the structural change of the molecules under the external electric field. It is noteworthy that the energy change of the PEGDME molecule is generally smaller than that of the PEG molecule, indicating that the PEGDME molecule is more stable under the reducing and

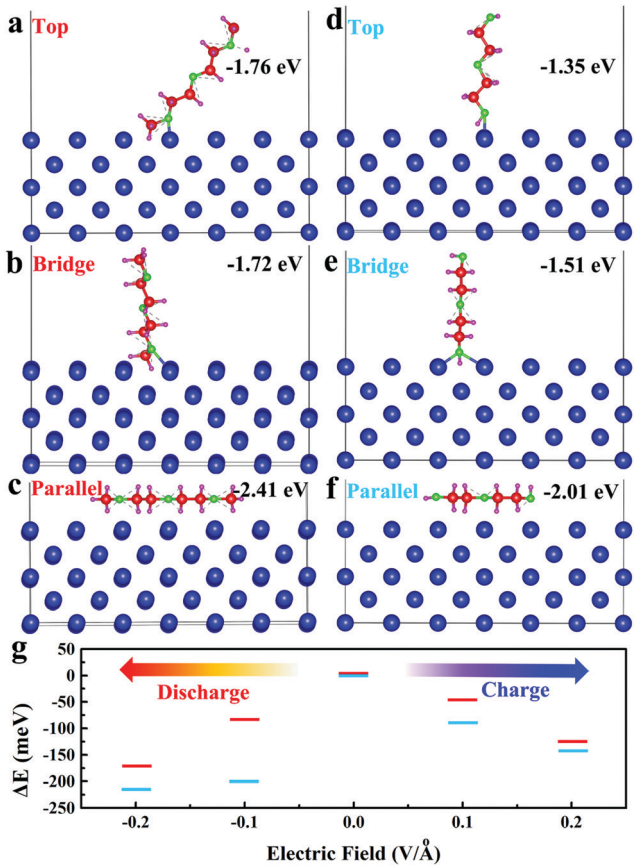

Fig. 4 Different adsorption sites on the Li(100) surface for the PEGDME molecule: (a) top, (b) bridge and (c) parallel. Different adsorption sites on the Li(100) surface for the PEG molecule: (d) top, (e) bridge and (f) parallel. (g) The total energy change of PEG and PEGDME induced by the electric field (blue line: PEG, red line: PEGDME).

oxidation environment, thus explaining the extended ESW of the PEGDME SPE.

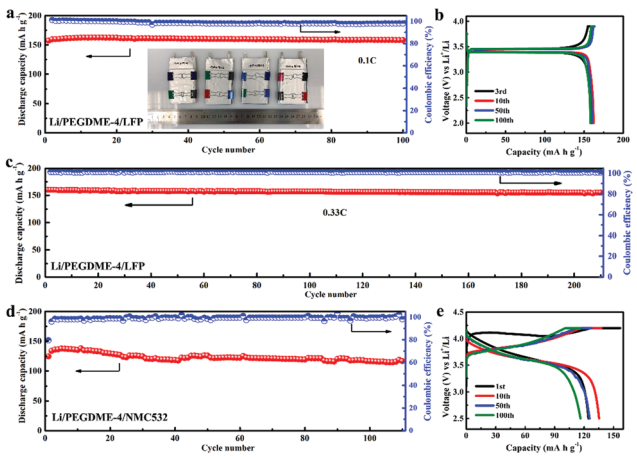

Fig. 5 Electrochemical performance of the PEGDME-4 SPE-based ASSLB pouch cells. (a) Cycling performance and (b) relative charge–discharge profiles of a Li/PEGDME-4/LFP cell at 0.1C. (c) Long-term cycling performance of the Li/PEGDME-4/LFP cell at 0.33C (LFP loading: 3.3 mg cm^{-2}). (d) Cycling performance and (e) relative charge–discharge profiles of a Li/PEGDME-4/NMC532 cell at 0.1C (NMC532 loading: 3.5 mg cm^{-2}).

As promising energy storage systems, ASSLBs are aimed at supplying energy to portable electronic devices and electric vehicles. Whether an associated technique is suitable for mass-production is therefore of significance. In order to investigate the commercial viability of the PEGDME-4 SPE, ASSLB pouch cells (inset of Fig. 5a) are evaluated. As shown in Fig. S27 (ESI†), the assembled Li-LFP pouch cell using the PEGDME-4 SPE and 3.3 mg cm^{-2} LFP can easily power an LED light. Moreover, the cells demonstrate excellent cycling stability, retaining capacities of 158.3 and 155.1 mA h g^{-1} after 100 and 210 cycles at 0.1C (Fig. 5a) and 0.33C (Fig. 5c) respectively. This corresponds to high capacity retentions of 98% and 97%, respectively. Further evidence for the excellent stability is evident from the almost overlapping charge–discharge curves in Fig. 5b. In like fashion to the coin cells, a Li-NMC532 pouch cell is tested in the voltage window from 2.5–4.2 V. Fig. 5d shows that with a loading of 3.5 mg cm^{-2}, the cell delivers a high capacity of 135 mA h g^{-1} after activation in the first two cycles, corresponding to an areal capacity of 0.47 mA h cm^{-2}. After 100 cycles, roughly 90% capacity retention is achieved with a capacity of around 120 mA h g^{-1}. The almost overlapping charge–discharge profiles in Fig. 5e and high CEs around 100% in Fig. 5d confirm the viability of our designed SPE for use in mass-produced high-voltage ASSLBs.

Conclusion

Here, PEG and PEGDME polymers are chosen to understand the limiting factor for the narrow ESW of PEO-based SPEs. The results demonstrated that the terminal –OH group in PEG will be first oxidized when the voltage is higher than 4.05 V, which is the main factor that limits the improvement of the ESW. Moreover, the reactive –OH group can react with the Li anode, which leads to poor Li stability. Replacing the reactive terminal –OH group with more stable $-OCH_3$ extends the ESW to 4.3 V and prolongs the life of Li–Li symmetric cells to over 2500 h (0.2 mA cm^{-2}, 0.2 mA h cm^{-2}). Benefitting from the enhanced Li anode stability and high voltage-resistance with the terminal $-OCH_3$ group, the assembled 0.53 mA h cm^{-2} Li-LFP pouch cell shows stable cycling for over 210 cycles at 0.33C with 97% capacity retention and CEs around 100%. A Li-NMC pouch cell with an areal capacity of 0.47 mA h cm^{-2} demonstrated over 90% capacity retention over 110 cycles in the operating voltage window from 2.5–4.2 V (0.1C). The findings of this work will encourage new opportunities for the realization of next-generation high-voltage ASSLBs.

Author contributions

X. Yang conceived and designed the experimental work and prepared the manuscript; X. Gao, C. Zhao, and J. Liang helped with SEM and XRD characterization; D. Bao, Y. Li and H. Huang helped with pouch cell assembly and performance testing; M. Jiang, S. Mukherjee and C. V. Singh designed and performed the DFT calculations and analysis; Q. Sun, N. Holmes, K. Adair, H. Duan, Q. Lu; W. Li, J. Li, L. Zhang and S. Lu participated in

the discussion of the data; R. Li purchased all chemicals; X. Sun supervised the overall project. All authors have given approval to the final version of the manuscript.

Conflicts of interest

There are no conflicts to declare.

Acknowledgements

This work was partly supported by the Natural Sciences and Engineering Research Council of Canada (NSERC), Canada Research Chair Program (CRC), Canada Foundation for Innovation (CFI), Ontario Research Fund, China Automotive Battery Research Institute Co., Ltd, Glabat Solid-State Battery Inc. and University of Western Ontario. C. V. Singh acknowledges additional support from Hart Professorship, Compute Canada, and University of Toronto. Qian Sun appreciates the support of MITACS Elevate postdoctoral program.

References

1 X. Yang, J. Luo and X. Sun, *Chem. Soc. Rev.*, 2020, DOI: 10.1039/C9CS00635D.
2 Q. Zhou, J. Ma, S. Dong, X. Li and G. Cui, *Adv. Mater.*, 2019, **31**, 1902029.
3 A. Manthiram, X. Yu and S. Wang, *Nat. Rev. Mater.*, 2017, **2**, 16103.
4 Y. Zhao, K. Zheng and X. Sun, *Joule*, 2018, **2**, 2583–2604.
5 E. Umeshbabu, B. Zheng and Y. Yang, *Electrochem. Energy Rev.*, 2019, **2**, 199–230.
6 J. Liang, J. Luo, Q. Sun, X. Yang, R. Li and X. Sun, *Energy Storage Mater.*, 2019, **21**, 308–334.
7 H. Xu, H. Zhang, J. Ma, G. Xu, T. Dong, J. Chen and G. Cui, *ACS Energy Lett.*, 2019, **4**, 2871–2886.
8 H. Zhang, J. Zhang, J. Ma, G. Xu, T. Dong and G. Cui, *Electrochem. Energy Rev.*, 2019, **2**, 128–148.
9 S.-J. Tan, X.-X. Zeng, Q. Ma, X.-W. Wu and Y.-G. Guo, *Electrochem. Energy Rev.*, 2018, **1**, 113–138.
10 J. Zhang, J. Yang, T. Dong, M. Zhang, J. Chai, S. Dong, T. Wu, X. Zhou and G. Cui, *Small*, 2018, **14**, 1800821.
11 X. Yang, X. Gao, C. Zhao, Q. Sun, Y. Zhao, K. Adair, J. Luo, X. Lin, J. Liang, H. Huang, L. Zhang, S. Lu, R. Li and X. Sun, *Energy Storage Mater.*, 2020, **27**, 198–204.
12 H. Huo, Y. Chen, J. Luo, X. Yang, X. Guo and X. Sun, *Adv. Energy Mater.*, 2019, **9**, 1804004.
13 J. Wan, J. Xie, X. Kong, Z. Liu, K. Liu, F. Shi, A. Pei, H. Chen, W. Chen, J. Chen, X. Zhang, L. Zong, J. Wang, L. Q. Chen, J. Qin and Y. Cui, *Nat. Nanotechnol.*, 2019, **14**, 705–711.
14 J. Ma, Z. Liu, B. Chen, L. Wang, L. Yue, H. Liu, J. Zhang, Z. Liu and G. Cui, *J. Electrochem. Soc.*, 2017, **164**, A3454–A3461.
15 H. Duan, M. Fan, W. P. Chen, J. Y. Li, P. F. Wang, W. P. Wang, J. L. Shi, Y. X. Yin, L. J. Wan and Y. G. Guo, *Adv. Mater.*, 2019, **31**, 1807789.
16 W. Zhou, Z. Wang, Y. Pu, Y. Li, S. Xin, X. Li, J. Chen and J. B. Goodenough, *Adv. Mater.*, 2019, **31**, 1805574.
17 C. Wang, T. Wang, L. Wang, Z. Hu, Z. Cui, J. Li, S. Dong, X. Zhou and G. Cui, *Adv. Sci.*, 2019, **6**, 1901036.
18 Q. Yang, J. Huang, Y. Li, Y. Wang, J. Qiu, J. Zhang, H. Yu, X. Yu, H. Li and L. Chen, *J. Power Sources*, 2018, **388**, 65–70.
19 S.-J. Kwon, D.-G. Kim, J. Shim, J. H. Lee, J.-H. Baik and J.-C. Lee, *Polymer*, 2014, **55**, 2799–2808.
20 Z. Lin and J. Liu, *RSC Adv.*, 2019, **9**, 34601–34606.
21 Y. C. Jung, M. S. Park, D. H. Kim, M. Ue, A. Eftekhari and D. W. Kim, *Sci. Rep.*, 2017, **7**, 17482.
22 T. M. Nguyen, J. Suk and Y. Kang, *J. Electrochem. Sci. Technol.*, 2019, **10**, 250–255.
23 K. M. Abraham, Z. Jiang and B. Carroll, *Chem. Mater.*, 1997, **9**, 1978–1988.
24 S. Gowneni and P. Basak, *J. Mater. Chem. A*, 2017, **5**, 12202–12215.
25 X. Fan, X. Ji, F. Han, J. Yue, J. Chen, L. Chen, T. Deng, J. Jiang and C. Wang, *Sci. Adv.*, 2018, **4**, eaau9245.
26 X. Fan, L. Chen, X. Ji, T. Deng, S. Hou, J. Chen, J. Zheng, F. Wang, J. Jiang, K. Xu and C. Wang, *Chem*, 2018, **4**, 174–185.
27 P. Yao, H. Yu, Z. Ding, Y. Liu, J. Lu, M. Lavorgna, J. Wu and X. Liu, *Front. Chem.*, 2019, **7**, 522.
28 H. Huo, Y. Chen, N. Zhao, X. Lin, J. Luo, X. Yang, Y. Liu, X. Guo and X. Sun, *Nano Energy*, 2019, **61**, 119–125.
29 X. Yang, Q. Sun, C. Zhao, X. Gao, K. R. Adair, Y. Liu, J. Luo, X. Lin, J. Liang, H. Huang, L. Zhang, R. Yang, S. Lu, R. Li and X. Sun, *Nano Energy*, 2019, **61**, 567–575.
30 X. Yang, X. Li, K. Adair, H. Zhang and X. Sun, *Electrochem. Energy Rev.*, 2018, **1**, 239–293.
31 D. Lin, P. Y. Yuen, Y. Liu, W. Liu, N. Liu, R. H. Dauskardt and Y. Cui, *Adv. Mater.*, 2018, **30**, 1802661.
32 D. Farhat, F. Ghamouss, J. Maibach, K. Edstrom and D. Lemordant, *ChemPhysChem*, 2017, **18**, 1333–1344.
33 C. Peebles, R. Sahore, J. A. Gilbert, J. C. Garcia, A. Tornheim, J. Bareño, H. Iddir, C. Liao and D. P. Abraham, *J. Electrochem. Soc.*, 2017, **164**, A1579–A1586.
34 X. Ma, R. S. Young, L. D. Ellis, L. Ma, J. Li and J. R. Dahn, *J. Electrochem. Soc.*, 2019, **166**, A2665–A2672.
35 Y. Qian, P. Niehoff, M. Börner, M. Grützke, X. Mönnighoff, P. Behrends, S. Nowak, M. Winter and F. M. Schappacher, *J. Power Sources*, 2016, **329**, 31–40.
36 M. Ebadi, C. Marchiori, J. Mindemark, D. Brandell and C. M. Araujo, *J. Mater. Chem. A*, 2019, **7**, 8394–8404.

